

Experimental Heat Transfer

A Journal of Thermal Energy Generation, Transport, Storage, and Conversion

ISSN: (Print) (Online) Journal homepage: <https://www.tandfonline.com/loi/ueht20>

Thermal management of an interventional medical device with double layer encapsulation

Nu Bich Duyen Do, Erik Andreassen, Stephen Edwardsen, Anders Lifjeld, Knut E. Aasmundtveit, Hoang-Vu Nguyen & Kristin Imenes

To cite this article: Nu Bich Duyen Do, Erik Andreassen, Stephen Edwardsen, Anders Lifjeld, Knut E. Aasmundtveit, Hoang-Vu Nguyen & Kristin Imenes (2021): Thermal management of an interventional medical device with double layer encapsulation, Experimental Heat Transfer, DOI: [10.1080/08916152.2021.1946208](https://doi.org/10.1080/08916152.2021.1946208)

To link to this article: <https://doi.org/10.1080/08916152.2021.1946208>



© 2021 The Author(s). Published with license by Taylor & Francis Group, LLC.



View supplementary material [↗](#)



Published online: 05 Jul 2021.



Submit your article to this journal [↗](#)



Article views: 333



View related articles [↗](#)



View Crossmark data [↗](#)

Thermal management of an interventional medical device with double layer encapsulation

Nu Bich Duyen Do^a, Erik Andreassen^{a,b}, Stephen Edwardsen^c, Anders Lifjeld^c, Knut E. Aasmundtveit^a, Hoang-Vu Nguyen^a, and Kristin Imenes^a

^aDepartment of Microsystems, University of South-Eastern Norway, Borre, Norway; ^bDepartment of Materials and Nanotechnology, SINTEF Industry, Oslo, Norway; ^cGE Vingmed Ultrasound AS, Horten, Norway

ABSTRACT

This paper presents a thermal study of a double-layer encapsulation for an interventional medical device, which operates temporarily inside the human esophagus for cardiac imaging. The surface temperature of test samples, representing the device, was assessed by experiments and numerical simulations. The test samples consisted of a heat source, a heat sink and a double-layer encapsulation consisting of a 3D printed biocompatible polymer (thickness 0.9 mm), with an electroplated Cu inner layer (0, 10, 80 or 150 μm thick). The surface temperature of test samples was measured in a tissue-mimicking thermal phantom at 37°C, with different heat source power levels. Experimental results showed that the maximum steady-state surface temperature could be reduced significantly by a 10 μm thick Cu layer (compared to no Cu layer). Increasing the Cu layer thickness further had a rather small effect, at least for low power levels. The maximum steady-state surface temperature was an exponential function of the Cu layer thickness. Test samples with a Cu electroplated polymer encapsulation and a heat source power of 0.5 W satisfied the maximum temperature limit for thermal safety (43°C) when the Cu layer was thicker than about 80 μm . Simulated surface temperatures were in good agreement with experimental values, for a model using two different thermal contact conductance coefficients (for different materials) for the sample-phantom boundary condition. The simulation model was also used to suggest alternative materials for the outer layer of an encapsulation with a metal inner layer, for reducing the surface temperature.

ARTICLE HISTORY



Received 4 March 2021
Accepted 16 June 2021

KEYWORDS


Interventional medical device; thermal safety; thermal management; heat transfer; metallized polymer encapsulation

Introduction

Ultrasound imaging plays an important role in the diagnosis of cardiovascular diseases. Imaging the heart with a probe inside the esophagus, known as trans-esophageal echocardiography (TEE), has the capability of providing high quality images of the heart. The TEE probe passes through the mouth of the patient into the esophagus, and provides 3D images of the heart in real time [1]. The tip of a TEE probe, referred to as ‘scan head’ in this paper, contains the ultrasound transducer and electronics. The thermal management of a TEE scan head is important with respect to patient safety, since the transducer and the electronics in the scan head generate heat during imaging. Therefore, the temperature distribution on the surface of the scan head must be well controlled to avoid hot spots. According to the standard for the safety and performance of ultrasonic medical diagnostic equipment, IEC 60601-2-37, the temperature of medical devices in contact with the patient for 10 minutes or more

CONTACT Kristin Imenes  Kristin.Imenes@usn.no  University of South-Eastern Norway, Department of Microsystems, Borre, Norway

This article has been republished with minor changes. These changes do not impact the academic content of the article.

 Supplemental data for this article can be accessed on the [publisher's website](#)

© 2021 The Author(s). Published with license by Taylor & Francis Group, LLC.

This is an Open Access article distributed under the terms of the Creative Commons Attribution-NonCommercial-NoDerivatives License (<http://creativecommons.org/licenses/by-nc-nd/4.0/>), which permits non-commercial re-use, distribution, and reproduction in any medium, provided the original work is properly cited, and is not altered, transformed, or built upon in any way.

must not exceed 43°C, to avoid thermal damage to biological tissue [2]. Thermal management is also critical for the performance, lifetime and reliability of the device [3, 4].

Thermal management of medical devices can be based on active solutions (requiring power, e.g. fans for forced convection, pumps for liquid cooling, refrigeration) or passive solutions (e.g. heat sinks, heat spreaders, heat pipes, vapor chambers, phase change materials) [3–5]. Technological advancements enable medical devices to become more compact. Hence, implementing solutions such as heat pipes, vapor chambers, fans, etc. for cooling the device will become more challenging due to the need of space. If the encapsulation of a device can act as an effective heat spreader to dissipate heat generated inside the device, this will be a compact solution.

Encapsulation of medical devices (e.g. TEE scan heads, and other implantable devices such as pacemakers, cochlear implants, implantable neuromuscular micro-stimulators, artificial retina implants) is often composed of two materials [3] to fulfill several functional requirements, not only related to thermal safety, but also electromagnetic interference (EMI) shielding, electrical isolation, and biocompatibility. Firstly, an electrically conductive material (e.g. a metallic material) provides EMI shielding [6] and heat transfer ability [7], due to high electrical and thermal conductivity. Secondly, an electrically insulating material (e.g. a polymeric or ceramic material) is responsible for electrical isolation and biocompatibility. The encapsulation can be built from several separate parts as in Figure 1 (with inner parts made of metals, and outer parts made of polymers or ceramics), or it can be a double-layer structure.

A double-layer encapsulation may be based on a metal part with a polymer or ceramic coating on the outside, or a polymer part metallized on the inside [8, 9]. In the first case, a thin film of a biocompatible polymer or ceramic covers the outside of a metal part. A metal part provides good heat spreading, EMI shielding and mechanical integrity for the encapsulation. However, an encapsulation with metal as the main material may be heavier than what is needed for the function. In addition, applying a uniform and smooth coating of a biocompatible polymer (e.g. parylene coating) or ceramic (e.g. Al_2O_3) on a metal part often requires complicated fabrication processes, such as chemical vapor deposition, or atomic layer deposition [9]. In the second case, the inner surface of a biocompatible polymer part is coated with a thin metal layer. This encapsulation concept utilizes the advantages of polymers, such as low density, easy and flexible processing, high electrical resistivity, and

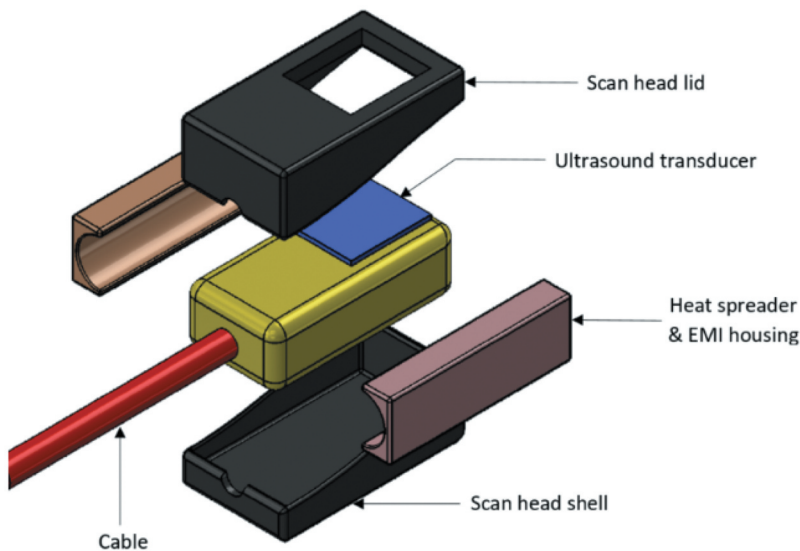


Figure 1. Schematic overview of the encapsulation of a TEE scan head, with metal parts for heat spreading and EMI shielding, and a biocompatible shell for sealing the device.

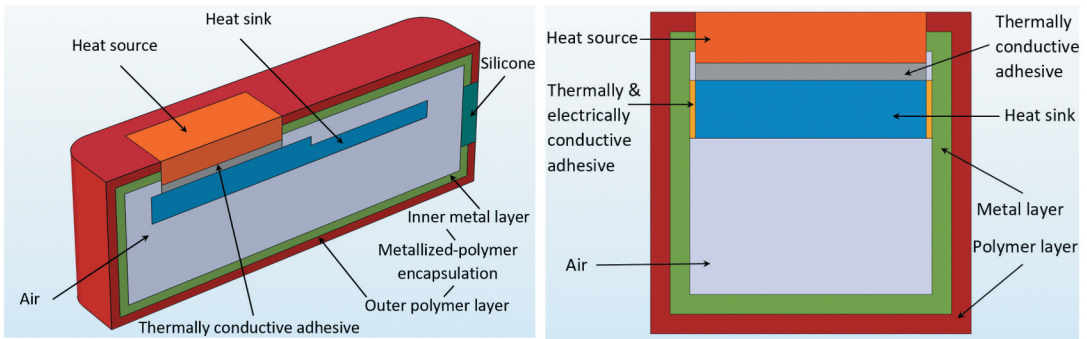


Figure 2. Schematic of cross-sections of the test sample (not drawn to scale), consisting of a heat source, a heat sink and a metallized polymer encapsulation.

low cost [10]. Additionally, a metallized polymer encapsulation can be fabricated by combining well-established industrial methods, such as e.g. injection molding for the polymer part, and metallization by vacuum metallization, electroless plating, electroplating, or even spray painting [4, 11]. A thin metal film (in the micro- or nanometer range) can provide enough EMI shielding for a TEE scan head and other non-radiation emitting medical devices [6, 12, 13]. However, for a metallized polymer encapsulation, the trade-off between metal and polymer thickness needs to be considered, so that the encapsulation can provide sufficient heat spreading, to avoid hot spots on the surface.

In a recent heat transfer simulation study [14], we compared the thermal performances of several TEE scan head encapsulation concepts. Ref [14], indicated that a metallized polymer encapsulation (as illustrated in Figure 2) can provide good heat spreading, and acceptable maximum surface temperature for low power levels. Hence, this article presents a detailed study of the thermal management of a scan head with a metallized polymer encapsulation. The main thermal requirement for a TEE scan head is that the maximum surface temperature must be below 43°C. In this article we study the effect of metal layer thickness (0, 10, 80, 150 μm of Cu) for a 0.9 mm thick polymer encapsulation, for different heat source power levels (0.5–2.0 W). To the best of our knowledge, this study is the first to investigate the role of a metallized polymer encapsulation for the thermal management of a TEE scan head. In addition, we present simulations that give insight on the heat transfer of the device, and provide a basis for establishing design rules and selecting material alternatives for the outer layer of the metallized encapsulation, in order to further improve the thermal performance of such devices.

Methodology

The sub-section “Experiments” describes the fabrication of the metallized polymer encapsulation, the preparation of test samples, and the temperature measurements in a tissue-mimicking phantom. The sub-section “Simulation of steady-state heat transfer” summarizes the model and approach for simulating the heat transfer of our device with metallized encapsulation. The third sub-section summarizes uncertainties in the experimental measurements and their effects on the parameters obtained by fitting simulations to experiments.

Experiments

Sample preparation

A simplified structure, representing the TEE scan head, was used for the thermal characterization. This test sample (with dimensions of about 37 mm \times 13 mm \times 12 mm) included a heat source, a heat sink and a metallized polymer encapsulation, as illustrated in Figure 2. The heat source represented electronic components generating heat within the scan head, such as the ultrasound transducer and

electronics. The geometry of the heat sink was similar to that in a commercial device. The metallized polymer encapsulation consisted of a thin metal layer deposited on the inner surface of the prefabricated polymer parts.

The encapsulation was fabricated by polymer 3D printing followed by electroplating. Two mating parts (one part corresponding to the half shown to the left in [Figure 2](#)) were 3D printed. A UV-cured polymer material was used with the 3D printer Stratasys Objet30 Prime, which is based on PolyJet 3D printing technology [15], belonging to the *material jetting* process category of additive manufacturing [16]. The biocompatible polymer material MED610 (from Stratasys) was selected, because the thermal properties of this material are similar to polymer encapsulation materials commonly used for interventional medical devices (e.g. the thermoplastic materials PEI and PEEK). MED610 also provides adequate electrical isolation and compatibility with biological tissue. A metal layer with desired thickness (10, 80, 150 μm) was deposited on the inner surfaces of the polymer parts (0.9 mm thick) by means of sputtering followed by electroplating. Copper (Cu) was chosen as the electroplating material due to its high thermal conductivity ($400 \text{ Wm}^{-1}\text{K}^{-1}$) [7], its effectiveness in EMI shielding [6], and its low cost. Furthermore, Cu electroplating is a common industrial process [11]. [Figure 3a](#) shows one encapsulation part after Cu electroplating. Details about the fabrication of the electroplated encapsulation are presented in the Supplementary Materials.

Based on preliminary electroplating trials, a polymer thickness of 0.9 mm was selected to ensure that the polymer part would not deform as a result of the electroplating. The thinnest Cu layer used in this study was 10 μm . This thickness will provide adequate EMI shielding effectiveness for the TEE scan head [6, 12, 13]. The thickest Cu layer in this study, 150 μm , was chosen in order to have a reasonable time for the electroplating process [11]. The standard deviation of the measured Cu thickness of the electroplated polymer part was about 10% (see Table S2 in the Supplementary Materials). Therefore, three Cu layer thicknesses (10, 80 and 150 μm) were used in this study, to evaluate the effect of metal thickness on the heat transfer.

The electroplated parts were subsequently assembled around a heat source and an aluminum (Al) heat sink to make a test sample representing a TEE scan head, as illustrated in [Figure 2](#) and [Figure 3](#). The heat source, a commercial resistive heating element (metal ceramic heater from Heat Scientific), was bonded to the heat sink using a thermally conductive adhesive (Epotek T7109-19), which was cured at 80°C for 2 hours. Two sides of the Al heat sink were attached to the Cu surfaces of the two encapsulation parts by thin layers of a thermally and electrically conductive adhesive (Epotek EJ2189-LV), which was cured at 40°C for 9 hours. This curing condition differed from the recommendation of the manufacturer (150°C , 1 hour) [17], in order to avoid thermally induced distortion of the polymer parts [18]. The hole for the electrical wires at the tail of the sample, and the seams between two mating electroplated parts, were sealed with a medical silicone, cured at 40°C for 6 hours. The remaining volume inside the sample (containing electronic components and cables in a typical scan head) was empty (air) for simplifying the simulations and representing a worst-case scenario with regards to heat transfer.

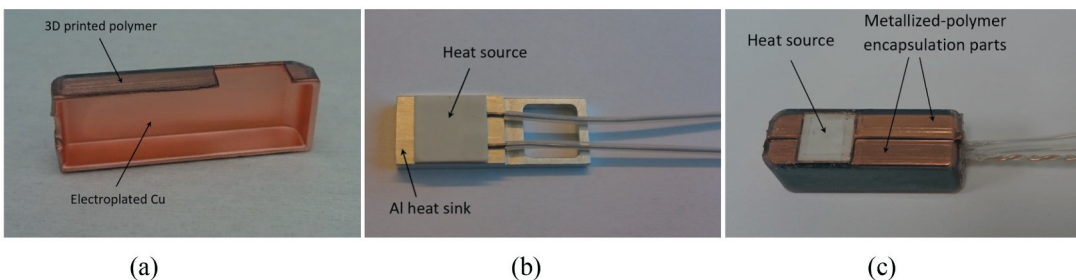


Figure 3. (a) Cu electroplated polymer part; (b) Heat source (resistive heating element) bonded to an Al heat sink; (c) Test sample after assembly.

Temperature measurements

The surface temperature of the test samples was measured for 80 minutes (about twice the duration of a common TEE exam [2, 19]), when placed in a tissue-mimicking thermal phantom (National Physical Laboratory, England), stabilized at around 37°C, see Figure 4. Test samples with 0, 10, 80 and 150 μm thick Cu layers were tested. The effect of the heat source power was also considered.

The thermal phantom is cylindrical with diameter 11 cm and height 11.5 cm. It is made of a tissue-mimicking material (TMM), prepared according to the standard IEC 60601-2-37. The TMM contains agar, glycerol, water and inorganic particles (e.g. SiC, Al₂O₃). Such thermal phantoms are commonly used for measuring ultrasound transducer surface temperature [2, 20, 21]. The acoustic and thermal properties are comparable to those of soft tissues [21]. Details about components and properties of the thermal phantom are given in ref [22]. When performing the temperature measurements in this study, the glycerol solution (which the phantom is stored in to prevent it from drying out) was removed to imitate the human esophagus environment. The test sample with attached thermocouples was carefully inserted into a cavity in the phantom (Figure 4), to avoid damaging the fragile phantom material. Note that some areas of the test sample surface were not in contact with the phantom, due to the thermocouples, the wires and the Kapton tape fixing the thermocouples (see Figure 5). The effect of

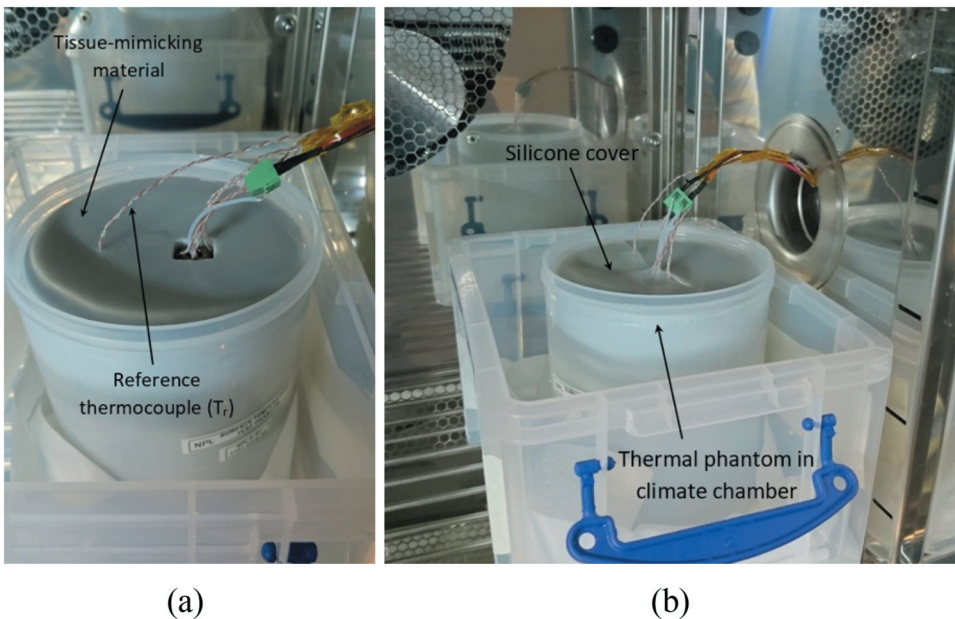


Figure 4. Test sample placed in a tissue-mimicking thermal phantom in a climate chamber.

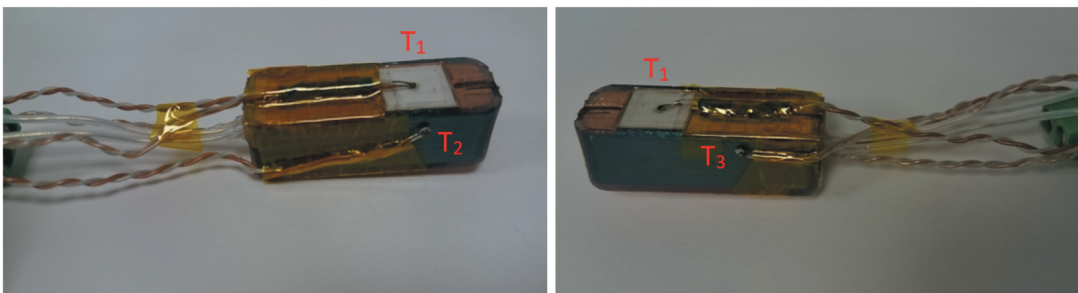


Figure 5. Thermocouples (T_1 , T_2 , T_3) on the surface of the test sample.

this is that the measured temperatures will be on the conservative side, due to the lower heat transfer to the phantom. However, also for a real scan head some surface areas may not be in contact with the tissue.

Before the test, the sample was kept in the phantom cavity for about 3 hours to stabilize at 37°C in the climate chamber. The end of the sample with the wires is facing up in the phantom (see [Figure 4a](#)), and this surface is not in contact with the phantom. The top surface of the phantom was covered by a sheet of silicone material (0.5 mm thick) during testing, as shown in [Figure 4b](#). This was for preventing the phantom material from drying out, and reducing the effect of air flow due to the fan in the climate chamber.

Type T thermocouples were positioned at three different locations on the test sample ([Figure 5](#)), in order to determine the maximum surface temperature during the test. Thermocouple T_1 is placed on the surface of the exposed heat source; thermocouple T_2 is placed on the vertical surface, near the heat source; thermocouple T_3 is placed on the other vertical surface, a bit further away from the heat source. The thermocouples were in contact with the sample surface via a thin layer of a thermal paste (Arctic MX-2), and they were fixed by Kapton tape. Note that these thermocouples measure a mixture of the sample surface temperature and the phantom temperature. However, the temperature measured at the heat source surface is dominated by the heat source, not the phantom, due to the heat source having the highest thermal effusivity. The temperature of the thermal phantom was also measured with a thermocouple (T_r in [Figure 4a](#)). The distance between the thermocouple T_r and the wall of the cavity in the thermal phantom was about 3.8 cm.

The thermocouples were logged (TC08 and PicoLog 6, PicoTech) every 10 s for 80 minutes. The heat source was connected to a power supply (R&S NGE100, Rohde & Schwartz), and four different power levels (0.5, 1.0, 1.5, 2.0 W) were used in the measurements. Five samples were fabricated and tested; two with Cu thickness 10 μm , one with 80 μm , one with 150 μm and one without Cu. For each sample, the temperature measurements were repeated twice (at all power levels), with 1 hour in between to let the sample return to 37°C.

Simulation of steady-state heat transfer

A simulation model, representing the experimental test sample ([Figure 2](#)) in the thermal phantom, was defined in COMSOL Multiphysics 5.3a. The heat source was modeled with uniform volumetric heat generation. The thermal conductivities of the materials in the model are listed in [Table 1](#). The thermal contacts between the components in the scan head were assumed to be perfect. The basis for this assumption is that metal-polymer thermal contact conductance (TCC) coefficients are on the order of $10^8 \text{ Wm}^{-2} \text{ K}^{-1}$ [30] and metal-metal TCC coefficients are even higher [30], and these conductances are

Table 1. Material properties of all components in the simulation model.

Component	Material	Thermal conductivity $k \text{ (Wm}^{-1} \text{ K}^{-1}\text{)}$
Heat source	Metal ceramic heater [23] (Al_2O_3 and W)	20
Heat sink	Al alloy 6082 [24]	180
Adhesive between heat source and heat sink	Thermally conductive adhesive (Epotek T7109-19) [25]	1.3
Adhesive between heat sink and encapsulation	Thermally and electrically conductive adhesive (Epotek EJ2189-LV) [17]	2.5
Inner layer of encapsulation	Electroplated Cu [26]	380
Outer layer of encapsulation	Polymer material (Stratasys MED610)	0.2 ^a
Coverage of the hole for the electrical wires	Medical silicone	0.2 ^a
Remaining volume inside the sample	Air [27]	$k(T)$ via COMSOL's material library

^aThermal conductivity selected based on common values from references [28, 29].

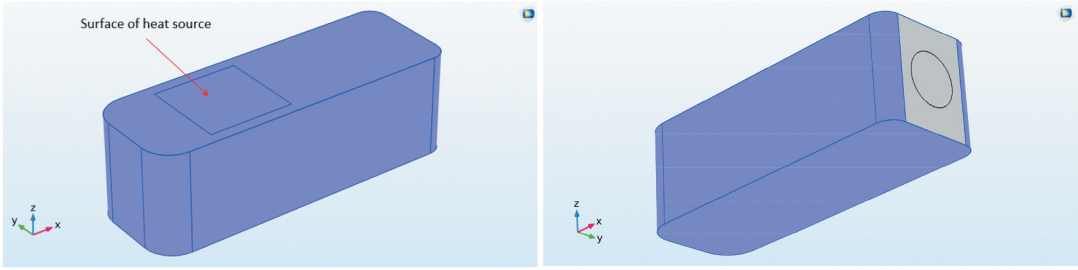


Figure 6. Illustration of thermal contact surfaces (in blue) for which Equation 1 was applied.

much larger than the conductance of the polymer layer in our model ($0.2 \text{ Wm}^{-1} \text{ K}^{-1} / 0.9 \text{ mm} \sim 10^2 \text{ Wm}^{-2} \text{ K}^{-1}$). For the outer surfaces of the scan head (in contact with the thermal phantom), a heat flux boundary condition with a TCC coefficient was applied:

$$q_0 = h_c(T_{ext} - T) \quad (1)$$

where h_c is the TCC coefficient; T_{ext} is the temperature of the phantom, (assumed to be constant, 37°C in our case); T is the temperature of the scan head surface; q_0 is the heat flux. The TCC coefficient is the inverse of the thermal contact resistance [31, 32]. Values for TCC coefficients were determined by comparing the simulated and measured steady-state surface temperatures, as detailed in the [section 3.2 Calibration of the simulation model](#).

The TCC coefficients mentioned above were used for the exterior of the scan head except the “tail” of the scan head (gray surface in [Figure 6](#)). In the experiment, this tail sees a small volume of air, i.e. the space between the encapsulation and the silicone lid covering the phantom’s cavity, see [Figure 4](#). The heat transfer coefficient for still air is often in the range $(2\text{--}25) \text{ Wm}^{-2} \text{ K}^{-1}$ [7]. A value of $15 \text{ Wm}^{-2} \text{ K}^{-1}$ was used in some simulations. However, including such a heat transfer coefficient for the tail of the scan head had no significant effect on the simulated maximum surface temperature (occurring at the un-encapsulated heat source). Hence, this extra heat transfer coefficient was not used in the results presented below.

The 3D model was meshed using free tetrahedral elements, see [Figure 7](#). The mesh had one element across the thin layers in the model (Cu and adhesive layers). An initial check with finer meshes (two elements across the thin layers, as well as an overall finer mesh with five times the number of elements) gave the same value for the maximum surface temperature, within 0.1 K. Hence, the mesh was

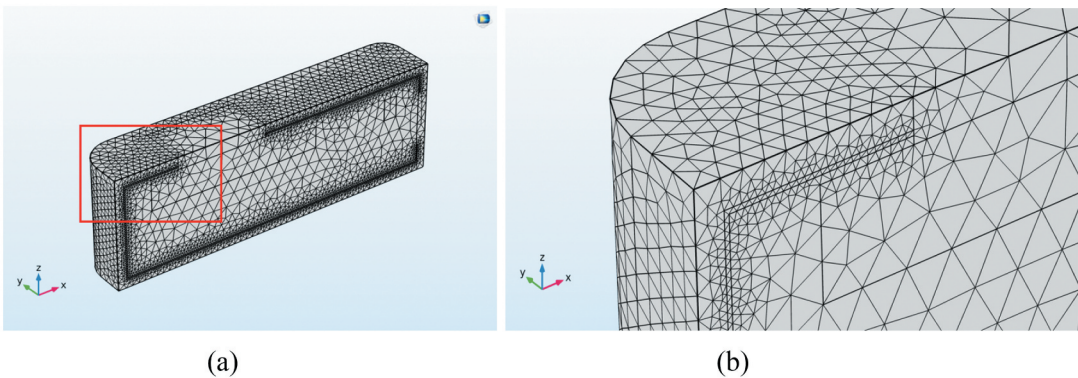


Figure 7. (a) Mesh on one half of the model, with a 0.9 mm thick polymer layer and a $150 \mu\text{m}$ thick Cu layer; (b) a zoom-in corresponding to the red rectangle in (a).

optimized with regard to simulation accuracy and calculation time. Details about the mesh are given in Table S3 in the Supplementary Materials.

Uncertainties and error calculations

What are the dominating uncertainties in the experimental measurements and how do these affect the parameters obtained by fitting simulations to experiments? Regarding the Cu thickness, the main source of uncertainty is the variation in Cu thickness over the sample, due to the deposition method. The Cu thickness was measured at 10–15 points on three cross-sections of the sample (altogether 40 points per sample, see Figure S1 in Supplementary materials). The average values were close to the nominal values ($\pm 1 \mu\text{m}$). The relative standard deviations were about 10%, i.e. for the $10 \mu\text{m}$ the standard deviation was $\pm 1 \mu\text{m}$. Details are given in Table S2 in Supplementary materials. The relative uncertainty in the polymer thickness is much smaller than that of the Cu thickness.

The power supplied to the test sample has an estimated uncertainty of about 1–2%, when the power is in the range of (0.5–2) W. This uncertainty estimate was determined using the uncertainty propagation law [33], based on the known uncertainties of voltage and current for the power supply used.

The variation in ΔT between repeated tests (with the same sample, not removed from the phantom, and with the same thermocouples mounted), was within the accuracy of the thermocouple used ($\pm 0.5^\circ\text{C}$); and that between two samples fabricated with the same nominal Cu thickness was within 1°C . Therefore, only measurements for one sample for each Cu thickness are presented in the Results section, as the example in Figure 8.

For comparison with simulations, steady-state temperatures of T_1 were estimated by fitting functions to the measured temperature transients of the 80 minute tests (as shown in Figure 8). Several functions, e.g. a power function, gave good fits to the experimental data. The difference between extrapolated values of the fitted function ($t \rightarrow \infty$) and experimental values at 80 minutes were small (lower than 0.3°C). Hence, the experimental values of T_1 at 80 minutes were used for calculating ΔT , and calibrating the simulation model.

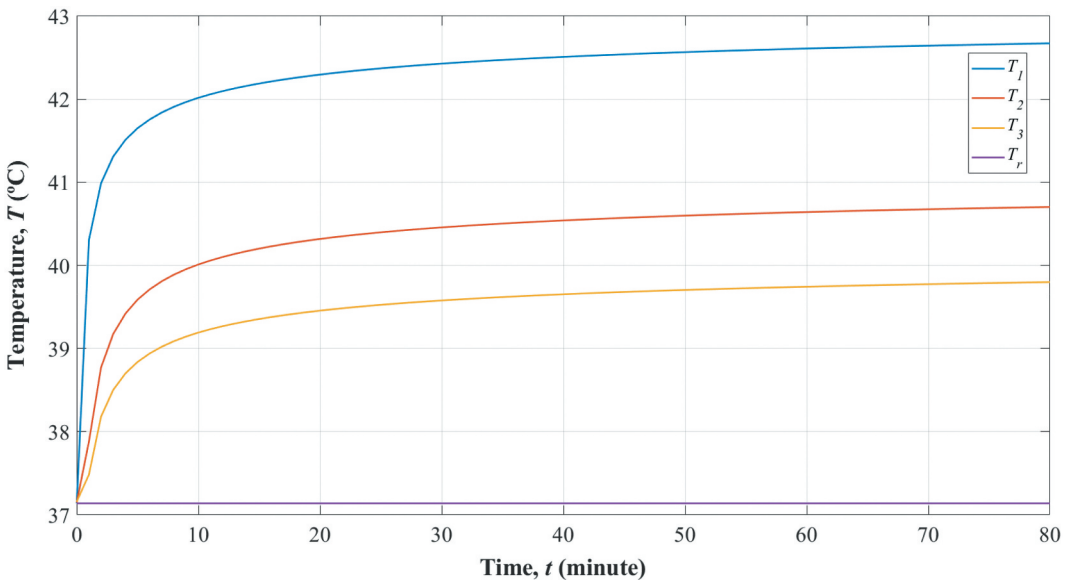


Figure 8. Measured temperatures for a test sample with polymer thickness 0.9 mm, Cu thickness $150 \mu\text{m}$, and heat source power 0.5 W. T_1 , T_2 , T_3 are surface temperatures measured at different positions (shown in Figure 5), and T_r is the temperature measured in the thermal phantom (shown in Figure 4).

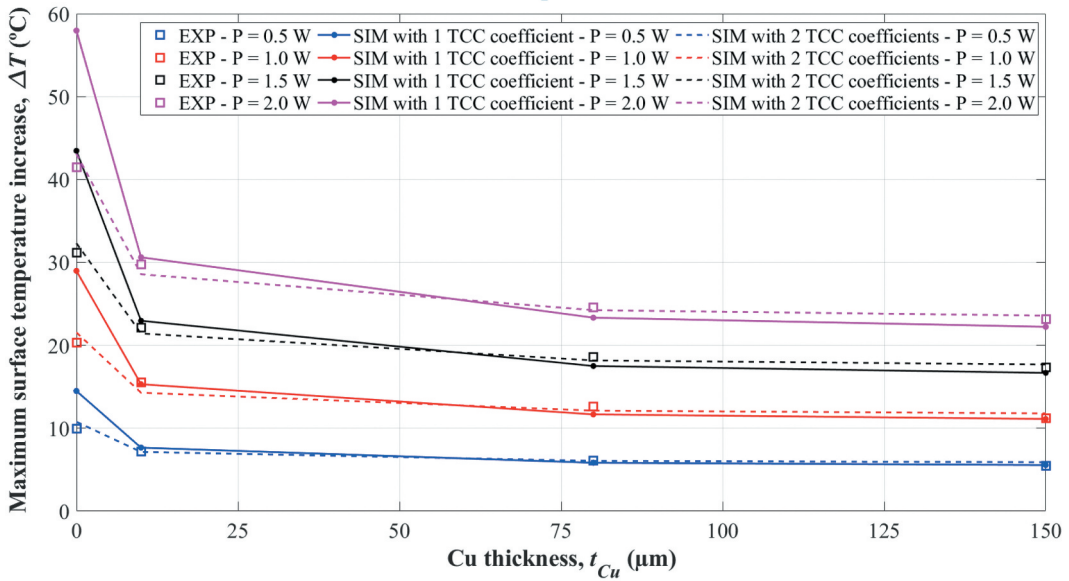


Figure 9. Simulated (SIM) and experimental (EXP) results for polymer encapsulations (0.9 mm) with 0, 10, 80 and 150 μm thick Cu layers, at different power levels. Experimental data are shown as squares, simulated data based on one TCC coefficient ($h_c = 75 \text{ Wm}^{-2}\text{K}^{-1}$) are shown as solid lines, and simulated data based on two TCC coefficients ($h_{c1} = 250 \text{ Wm}^{-2}\text{K}^{-1}$ and $h_{c2} = 46 \text{ Wm}^{-2}\text{K}^{-1}$) are shown as dashed lines.

When calibrating the simulation model by adjusting the two TCC coefficients (as in Figure 9), the uncertainties of the TCC coefficients h_{c1} and h_{c2} are $12 \text{ Wm}^{-2}\text{K}^{-1}$ and $4 \text{ Wm}^{-2}\text{K}^{-1}$, respectively. This is an estimate based on the dominating experimental uncertainties given above, as well as a requirement that systematic errors (differences between experimental and simulated ΔT) vs. Cu thickness should be minimized.

Results and discussion

Experimental results

As described in the introduction, the surface temperature limit for medical devices in contact with the human body for 10 minutes or more is 43°C . Hence, our study focuses on the maximum surface temperature, and how it varies with Cu layer thickness (0, 10, 80, 150 μm) and heat source power (0.5, 1.0, 1.5, 2.0 W).

Figure 8 shows temperature measurements for a case with 0.5 W power, and an encapsulation with polymer thickness 0.9 mm and Cu thickness 150 μm . After about one hour, the system is close to steady state. As expected, the maximum surface temperature of the test sample appears on the surface of the heat source (which is exposed, not encapsulated), shown as T_1 in Figure 5 and Figure 8. On the vertical exterior surfaces of the encapsulation, thermocouple T_2 shows a higher temperature than thermocouple T_3 . This is due to T_2 being closer to the heat source of the test sample, as shown in Figure 5.

We define ΔT as the difference between the maximum scan head surface temperature (T_1) and the temperature of thermal phantom (T_r), at steady state. Relationships between the measured ΔT and the Cu layer thickness (t_{Cu}), for different power levels (P), are shown in Figure 9 and Figure 10. ΔT increases linearly with increasing power because we consider steady state temperatures. Furthermore, ΔT decreases with increasing Cu thickness (better heat spreading), following an exponential function, as shown in Figure 10. The experimental results for this simplified test sample (Figure 9 and Figure 10)

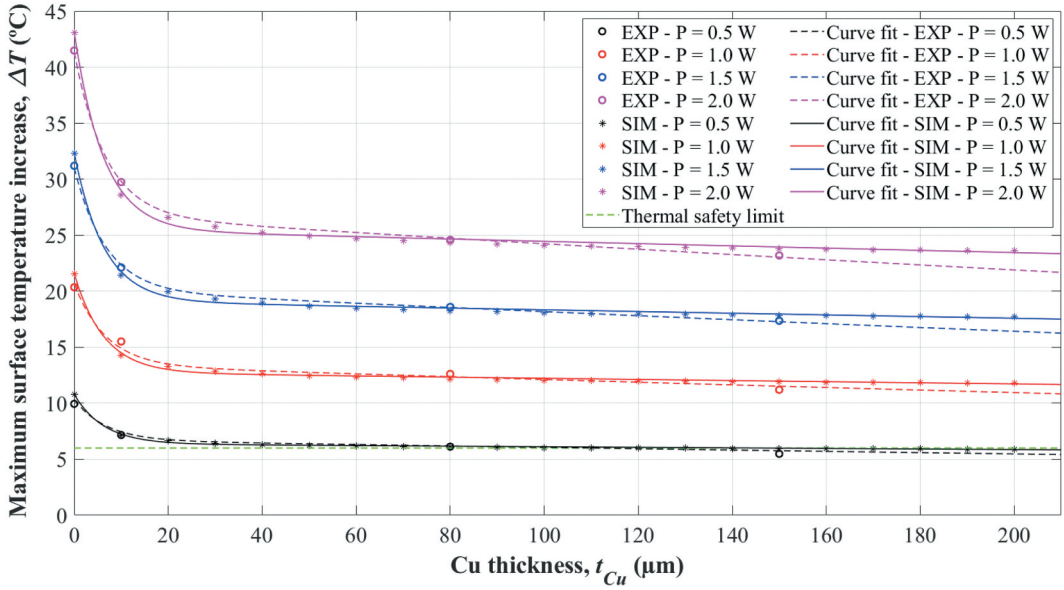


Figure 10. The relationship between the Cu layer thickness (t_{Cu}) and the increase in surface temperature above the phantom temperature at steady state (ΔT), for four different power levels (P). Dashed lines are fits (based on Equation 2) to experimental data (EXP, open circles), while solid lines are corresponding fits to simulations (SIM, asterisks). The thermal safety limit corresponds to $\Delta T = 6^\circ\text{C}$ (green dashed line).

show which combinations of Cu layer thickness and power that satisfy the temperature criterion ($T_1 < 43^\circ\text{C}$, i.e. $\Delta T < 6^\circ\text{C}$). For the examined combinations and a power level of 0.5 W, it is satisfied when the Cu layer is thicker than about 80 μm . Figure 10 also shows that increasing the Cu thickness from 80 to 150 μm has a small effect on ΔT . For a power level of 0.5 W, a Cu layer thickness around 100 μm (on a 0.9 mm thick polymer encapsulation) may be a good trade-off between thermal performance and cost/time for the metallization process.

Calibration of the simulation model

With the thermal conductivities in Table 1, the simulation model was first calibrated with the experimental data (ΔT vs. Cu thickness and heat source power, i.e. 16 data points) by adjusting a single TCC coefficient (h_c). With a h_c value of $75 \text{ Wm}^{-2} \text{ K}^{-1}$, the simulated ΔT values agreed well with the experimental data of samples having a non-zero Cu layer thickness. However, the ΔT values of the samples without Cu were grossly overestimated, as shown in Figure 9 (solid lines). Alternatively, a h_c value could be found so that ΔT values for zero Cu samples agreed with experiments, but then the ΔT values for non-zero Cu samples were underestimated. Hence, the balance between the two main thermal flow paths, “directly” through the heat source and via the encapsulation, was obviously poorly modeled. To try to obtain a good agreement for the entire dataset, the values for the thermal conductivities of the parts in the scan head were varied (within reasonable limits), while also varying the TCC coefficient. However, the overprediction mentioned above remained gross. A situation with only random errors (due to unavoidable uncertainties in the experimental values), and no systematic errors related to the presence of a Cu layer or not, could not be obtained. Furthermore, the areas for thermal contact with the phantom, on different surfaces of the scan head, were also varied, in an attempt to be closer to the experimental situation (some areas shielded from contact by wires, etc.). However, the overall prediction remained poor, with a systematic error related to the presence of a Cu layer, and not only random errors.

As a next step in trying to improve the prediction, we allowed for having two different TCC coefficients; h_{c1} for the heat source (modeled as Al_2O_3) surface and h_{c2} for the remainder of the scan head surface (the polymer encapsulation). A TCC coefficient accounts for effects of e.g. surface roughness at the interface, but it is evidently also related to bulk properties of the contacting materials, such as the thermal conductivity [32, 34]. Hence, we argue that the heat source and the polymer encapsulation, with thermal conductivities differing by a factor 100 and also different surface roughnesses, can have different TCC coefficients. However, these coefficients also effectively account for differences in contact area/pressure toward the thermal phantom.

A good overall fit was achieved with h_{c1} and h_{c2} set to $250 \text{ Wm}^{-2} \text{ K}^{-1}$ and $46 \text{ Wm}^{-2} \text{ K}^{-1}$, respectively, see [Figure 9](#) and [Figure 10](#), and these coefficients were used in all simulations reported in [Figure 10](#) and later. However, note that the simulations underpredict the (small) reduction in ΔT when increasing the Cu thickness from 80 to 150 μm , see [Figure 10](#). The remaining, rather small, difference between simulated and experimental data can be explained by various factors. One factor could be in the experimental data themselves. As mentioned in the experimental section, the thermocouple on the heat source measures a mix of the sample surface temperature and the phantom temperature. The mixing ratio may depend on the temperature, hence, e.g. the Cu layer thickness. Another factor could be that the idealized simulation model did not take into consideration the variation in the Cu layer thickness (about 10%, as presented in Table S2 in the Supplementary Materials). In addition, the thickness of the adhesive layers in the test samples may vary somewhat from sample to sample due to the manual assembly, but a constant thickness is assumed in the simulation model.

It is relevant to compare the TCC coefficients found above with the convective heat transfer coefficients for the human esophagus determined experimentally by Liao et al. [35]. Liao et al. investigated the heat transfer properties of the esophagus wall, as an indication of segmental blood flow changes during mechanical distension. The device used in their set-up was an ultrasound probe with a polyurethane bag attached to its tip. They found the heat transfer coefficient to be in the range $100\text{--}220 \text{ Wm}^{-2} \text{ K}^{-1}$, depending on the blood flow rate as affected by distension temperature. We interpret their results to indicate that the heat transfer coefficient of the esophagus wall was around $150 \text{ Wm}^{-2} \text{ K}^{-1}$ at body temperature.

Simulation results

The simulated ΔT values (using the two TCC coefficients given in the preceding [Section 3.2](#) Calibration of the simulation model), as well as the experimental data, were well represented by an exponential function:

$$\Delta T = (ae^{bt_{Cu}} + ce^{dt_{Cu}})P \quad (2)$$

where a , b , c , d are fitting parameters, t_{Cu} is the Cu thickness and P is the heat source power. Details about the fitting parameters for the simulated ΔT and the experimental ΔT are presented in the Supplementary Materials. [Figure 10](#) shows the maximum surface temperature increase as a function of Cu thickness at different power levels.

The simulation model can be used to visualize the temperature distributions. An example is shown in [Figure 11](#). In this case the encapsulation has a Cu layer thickness of 150 μm , and the heat source power is 0.5 W. The surface temperature varies from 39.9°C to 42.9°C. The maximum surface temperature occurs at the surface of the heat source, which is not encapsulated. The maximum surface temperature here satisfies the safety requirement; i.e. no spots on the surface are hotter than 43°C.

[Figure 12](#) shows simulated temperature distributions for different encapsulations, with Cu (a) and without Cu (b and c). There is a clear difference between encapsulations with and without Cu, regarding the balance between the two main heat flow paths to the phantom; the main path through

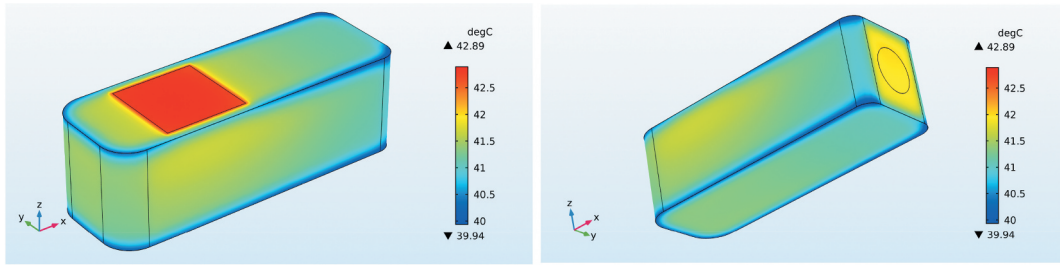
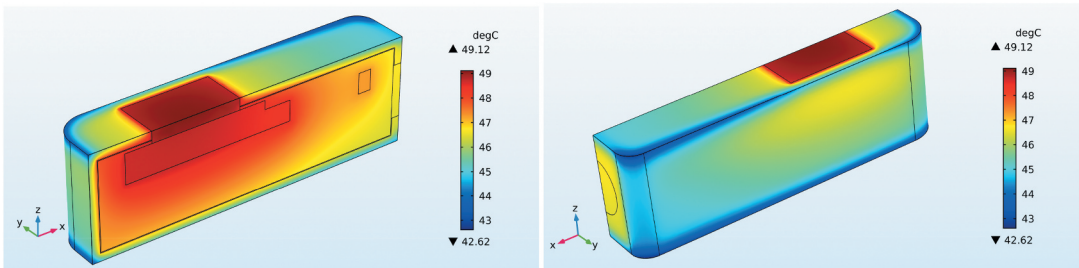
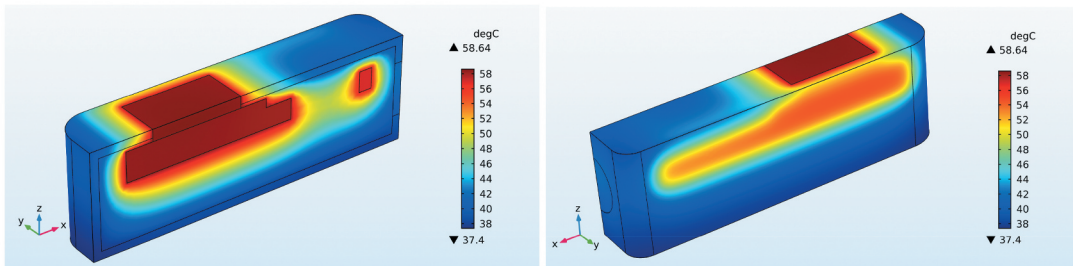


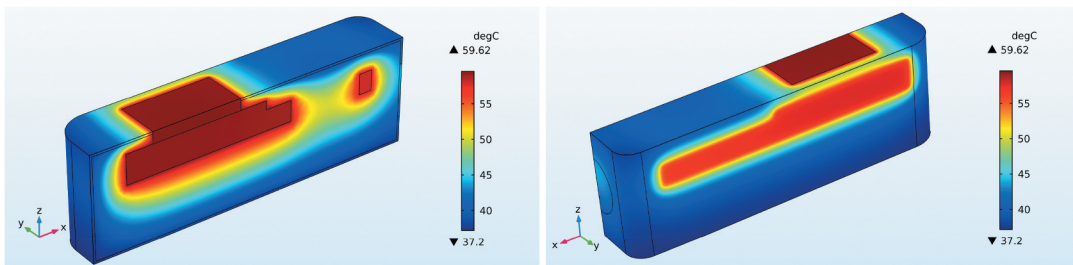
Figure 11. Simulated surface temperature. The outer polymer thickness is 0.9 mm, the inner Cu layer is 150 μm thick, and the heat source power is 0.5 W.



(a)



(b)



(c)

Figure 12. Simulated temperature distributions for three different encapsulations (1 W in all cases) (a) 0.9 mm thick polymer layer and 80 μm thick Cu layer (temperature range: 42.6–49.1°C); (b) 0.9 mm thick polymer layer and no Cu layer (temperature range: 37.4–58.6°C); (c) 0.25 mm thick polymer layer and no Cu layer (temperature range: 37.2–59.6°C).

the heat source “window” (with area 1 cm^2) and the secondary path through the polymer encapsulation. The secondary flow path is more pronounced when the encapsulation has a Cu layer, due to better heat spreading. The balance between these two paths can also be assessed by the relative heat flow through the heat source window. This relative heat flow is 30% in [Figure 12a](#), and 54% in

Figure 12b. The heat flux is almost constant over this window. Hence, a plot of relative heat flow vs. Cu thickness is similar to a plot of ΔT vs. Cu thickness. (However, the relative heat flow is independent of power level, since we consider the steady state.)

Figure 13 shows the simulated relationship between the polymer layer thickness (t_{po}) and the maximum surface temperature increase (ΔT), for different Cu thickness, at a power level of 0.5 W. Note that the simulation model was parameterized with the outer dimensions fixed, and a reduction in polymer thickness had to be compensated for by an increase in the thickness of the adhesive layer (between the Al heat sink and the encapsulation). However, this had no effect on the trends in this figure. As a check of this, some simulations were performed in which the thermal conductivity of the adhesive was increased from its nominal value ($2.5 \text{ Wm}^{-1}\text{K}^{-1}$) to the value of the Al heat sink ($180 \text{ Wm}^{-1}\text{K}^{-1}$). Results from these simulations are shown as a dashed green line. For a given Cu thickness, ΔT increases with increasing polymer thickness, due to the increasing thermal insulation of the thermal flow path through the encapsulation. However, the effect of the polymer thickness is small in this interval (0.25–1 mm), and it decreases with decreasing Cu thickness. For a very thin Cu layer (e.g. $2 \mu\text{m}$ Cu in Figure 13), the effect of polymer thickness on ΔT is negligible. When there is no Cu layer, ΔT decreases slightly with increasing polymer thickness (also seen in Figure 12c vs. Figure 12b), due to the increased heat spreading in the (thicker) polymer layer, dominating over the increased thermal insulation. When the polymer thickness is increased, the increased in-plane heat spreading in the polymer layer (typically occurring near the heat source and the heat sink) prevails over the reduced heat flow perpendicular to the polymer wall.

The simulations show that this scan head design and encapsulation concept satisfies the thermal criterion ($\Delta T < 6^\circ\text{C}$) for power levels up to about 0.5 W. In order to use a Cu plated encapsulation at higher power levels, the polymer must be replaced by a material with higher thermal conductivity. Our simulation model can be used to evaluate the effect of increased thermal conductivity of the outer layer. However, the model is probably not valid for materials

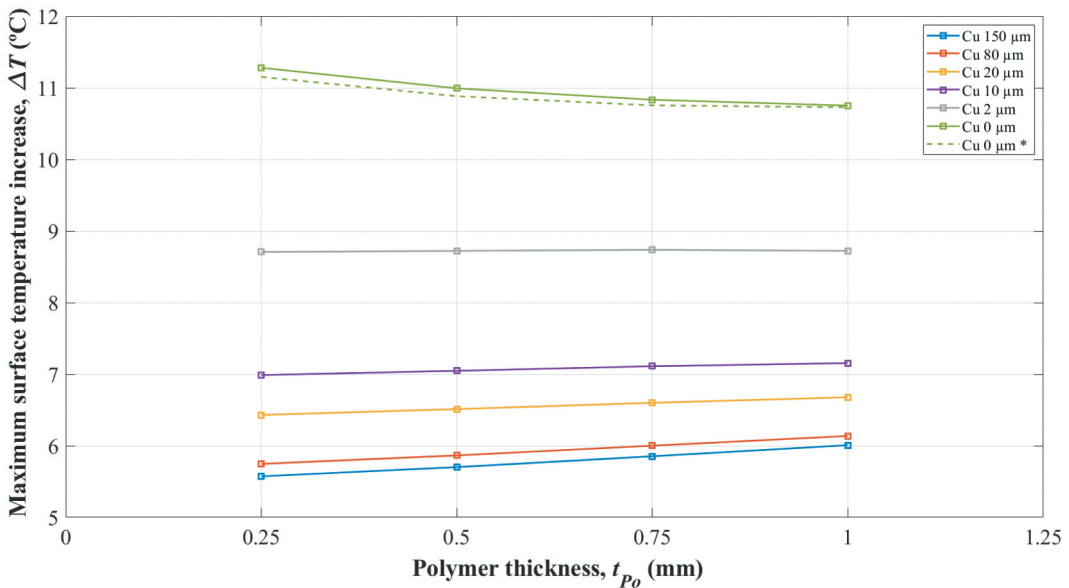


Figure 13. Simulated effect of polymer layer thickness (t_{po}) on the surface temperature increase (ΔT) for different Cu layer thicknesses. The heat source power was 0.5 W in these simulations. The dashed green line represents a case in which the thermal conductivity of the adhesive (between the Al heat sink and the encapsulation) was increased from its nominal value ($2.5 \text{ Wm}^{-1}\text{K}^{-1}$) to the value of the Al heat sink ($180 \text{ Wm}^{-1}\text{K}^{-1}$).

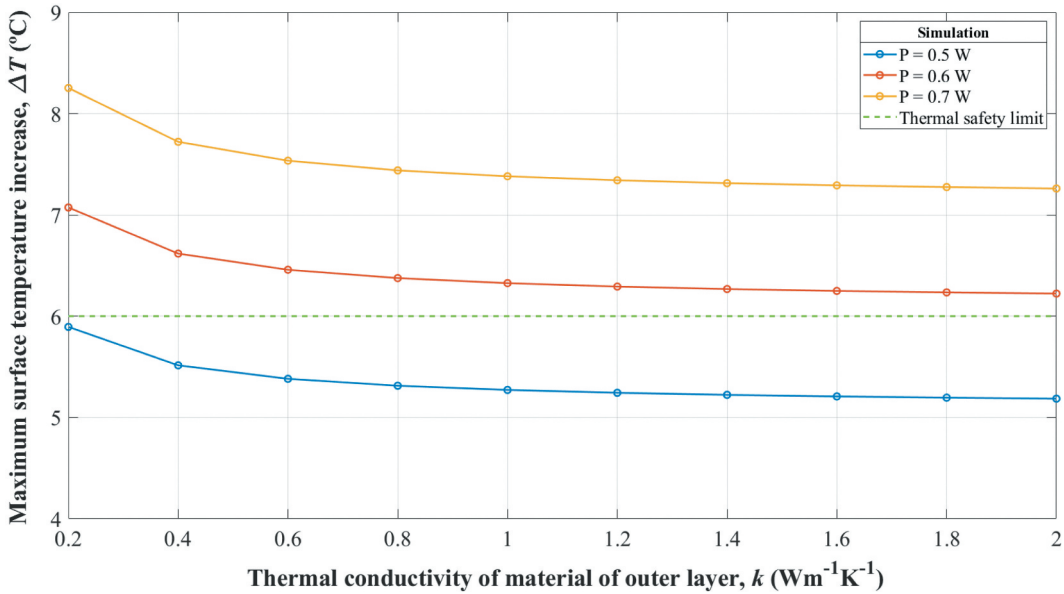


Figure 14. Simulated effect of the thermal conductivity (k) of the outer layer material on the maximum surface temperature increase (ΔT), for different power levels. The polymer outer layer is 0.9 mm thick, and the Cu inner layer is 150 μm thick.

with much higher thermal conductivity than the one used in the calibration. Figure 14 shows the simulated effect of the thermal conductivity (k) of the outer layer material on the maximum surface temperature increase (ΔT), for different power levels (P). Increasing the thermal conductivity from 0.2 to 2 $\text{Wm}^{-1}\text{K}^{-1}$ reduces ΔT by about 1°C.

Simulations with extreme values for the polymer thermal conductivity can be used to assess the thermal limits of a scan head design. If the polymer has zero thermal conductivity, all the heat transfer to the phantom will be through the 1 cm^2 “window” of the heat source, with or without a Cu layer on the polymer part. As an example (see Figure S2 in the Supplementary Materials), for a power of 1 W this would give a ΔT value of 40.0°C. In the other limit, for very high polymer thermal conductivities, ΔT approaches about 9.8°C (for 1 W power), with or without Cu. This corresponds to a heat flow fraction through the heat source window of about 0.25. This is then a value characterizing this particular design. Hence, with 1 W power, the temperature criterion, $\Delta T \leq 6^{\circ}\text{C}$, can not be reached with this design.

Material selection for the outer layer

This metallized encapsulation can only be used at power levels above 0.5 W if the polymer of the Cu electroplated encapsulation is replaced by a material with higher thermal conductivity. Polymer-based composites with fillers with high thermal conductivity can be taken into consideration for the outer layer of a metallized encapsulation. Such a composite should also fulfill other safety requirements, such as electrical isolation and biocompatibility. An advantage of using a polymer-based composite is the compatibility of this material type with well-developed packaging techniques, such as molding processes (e.g. injection molding, transfer molding, or compression molding) [4]. Composites based on a biocompatible polymer matrix and thermally conductive and electrically insulating fillers are promising candidates. The polymer could be a thermoset (e.g. biocompatible epoxy or silicone) or a thermoplastic (e.g. PEI or PEEK) [29]. Common thermally conductive and electrically insulating fillers are ceramic fillers; for example, metal oxides (e.g. alumina (Al_2O_3) or quartz (crystalline SiO_2)), or non-oxide fillers (e.g. aluminum nitride (AlN), boron nitride (BN), silicon nitride (Si_3N_4)) [10].

Ohashi et al. [36] successfully prepared a polymer composite with thermal conductivity of $8.2 \text{ Wm}^{-1}\text{K}^{-1}$ from epoxy with 74 vol% AlN. The composite was applied in fabricating encapsulants for dissipating the heat generated in electronic devices. Thermal conductivity of $21.3 \text{ Wm}^{-1}\text{K}^{-1}$ was achieved for an epoxy/BN composite in a study by Zhu et al. [37]. Kusunose et al. [38] measured a thermal conductivity of $9.2 \text{ Wm}^{-1}\text{K}^{-1}$ for an epoxy composite with 60 vol% Si_3N_4 nanowires. Biocompatible ceramics can also be considered as outer layer materials for the metallized encapsulation. The outer encapsulation can e.g. be fabricated by powder injection molding using AlN (100–300) $\text{Wm}^{-1}\text{K}^{-1}$ [10, 39, 40].

Conclusions

In this paper, the thermal management of a simplified trans-esophageal echocardiography (TEE) scan head was studied by experimental work and numerical simulations. Scan head test samples with a metallized polymer encapsulation were fabricated. The encapsulation consisted of a 3D printed polymer part with a Cu layer electroplated on the inside. The focus of the study was to investigate encapsulation parameters, with regards to the requirement that the maximum surface temperature of the scan head (in contact with human tissue) must be below 43°C .

Samples with encapsulations having a 0.9 mm thick polymer outer layer, and an electroplated Cu inner layer (0, 10, 80 or 150 μm thick), were tested with different power levels (0.5–2.0 W) supplied to the heat source in the sample. The heat source was connected to some sections of the encapsulation via an aluminum heat sink. The surface temperature of the test sample was measured in a tissue mimicking thermal phantom, which was stabilized at around 37°C (human body temperature) in a climate chamber.

Experimental results showed that the maximum steady-state surface temperature could be reduced significantly by a 10 μm thick Cu layer (compared to no Cu layer). Increasing the Cu layer thickness further had a rather small effect, at least for low power levels. The maximum steady-state surface temperature was an exponential function of the Cu layer thickness. As expected for this steady-state temperature, it increased linearly with increasing power supplied to the sample. Test samples with a Cu electroplated polymer encapsulation and a heat source power of 0.5 W satisfied the maximum temperature requirement ($< 43^\circ\text{C}$) when the Cu layer was thicker than about 80 μm .

A finite element model, for steady-state thermal simulations, was calibrated with the temperature measurements. In order to obtain a good prediction of all experiments, with and without a Cu inner layer, two thermal contact conductance coefficients were needed for the boundary conditions of the scan head exterior surface (toward the thermal phantom); one coefficient for the un-encapsulated heat source ($250 \text{ Wm}^{-2}\text{K}^{-1}$) and one for the polymer encapsulation ($46 \text{ Wm}^{-2}\text{K}^{-1}$). With this calibration, simulated steady-state temperatures were in good agreement with the experiments, i.e. for all Cu layer thicknesses and power levels. The simulation model was used to suggest material properties for the outer layer that can allow for higher power levels. The preferred outer material is a biocompatible and electrically insulating material with high thermal conductivity, e.g. a biocompatible ceramic or a thermally conductive and electrically insulating polymer composite.

The simulation model in this paper enables quick computations to evaluate the thermal management of TEE scan head designs with (double layer) metallized encapsulation. Further work is needed to extend the validity of the model to a wider range of encapsulation materials, and to establish a more fundamental physical description of the heat transfer from the TEE scan head to the thermal phantom, and to the tissue of the human esophagus. A more comprehensive model should include the thermal phantom (or the human tissue) in the computational domain, and the simulation should be transient.

Nomenclature

h_c	thermal contact conductance coefficient ($\text{Wm}^{-2} \text{K}^{-1}$)
h_{c1}	thermal contact conductance coefficient for the heat source ($\text{Wm}^{-2} \text{K}^{-1}$)
h_{c2}	thermal contact conductance coefficient for the external surfaces of the encapsulation of the test sample in contact with the phantom surface ($\text{Wm}^{-2} \text{K}^{-1}$)
k	thermal conductivity of a material ($\text{Wm}^{-1} \text{K}^{-1}$)
P	power supplied to the heat source of the test sample (W)
q_0	heat flux (Wm^{-2})
T	simulated temperature of the surface of the TEE scan head ($^{\circ}\text{C}$)
T_{ext}	simulated temperature of the thermal phantom ($^{\circ}\text{C}$)
T_1	measured temperature of the thermocouple placed on the heat source surface in the test sample ($^{\circ}\text{C}$)
T_2	measured temperature of the thermocouple placed on the vertical surface of the encapsulation, near the heat source ($^{\circ}\text{C}$)
T_3	measured temperature of the thermocouple placed on the vertical surface of the encapsulation, far from the heat source ($^{\circ}\text{C}$)
T_r	measured temperature of the thermocouple placed in the thermal phantom ($^{\circ}\text{C}$)
ΔT	difference between T_1 and T_r ($^{\circ}\text{C}$); i.e. $\Delta T = T_1 - T_r$
t	measurement time (s)
t_{Cu}	thickness of the Cu layer in the metallized encapsulation (m)
t_{po}	thickness of the polymer layer in the metallized encapsulation (m)
a, b, c, d	fitting parameters

Acknowledgments

This work was funded by the Research Council of Norway through the BIA program (grant number: 269618; *Mechanical miniaturization in interventional medical instruments*), and by the Norwegian Micro- and Nano-Fabrication Facility (NorFab, project number: 245963/F50). The authors gratefully acknowledge Mrs. Zekija Ramic, Mr. Svein Mindrebøe, Dr. Thai Anh Tuan Nguyen and Mr. Thao Ngoc Vo at the University of South-Eastern Norway (USN) for their assistance with laboratory work. We sincerely thank Dr. Helge Kristiansen at Conpart AS, Prof. Tao Dong and Dr. Zhongyuan Shi at USN for valuable discussions.

Disclosure statement

No potential competing interest was reported by the authors.

Funding

This work was funded by the Research Council of Norway through the BIA program (grant number: 269618; *Mechanical miniaturization in interventional medical instruments project*), and by the Norwegian Micro- and Nano-Fabrication Facility (NorFab, project number: 245963/F50).

Data availability statement

The raw/processed data required to reproduce these findings cannot be shared at this time due to legal restrictions.

References

- [1] E. C. Pua, S. F. Idriss, P. D. Wolf, and S. W. Smith, "Real-time 3D transesophageal echocardiography," *Ultrason. Imaging.*, vol. 26, no. 4, pp. 217–232, 2004. DOI: [10.1177/016173460402600402](https://doi.org/10.1177/016173460402600402).
- [2] IEC, IEC 60601-2-37 - Particular requirements for the safety of ultrasonic medical diagnostic and monitoring equipment, 2004.
- [3] R. Bahru, A. A. Hamzah, and M. A. Mohamed. "Thermal management of wearable and implantable electronic healthcare devices: perspective and measurement approach," *Int. J. Energy Res.*, 2020. DOI: [10.1002/er.6031](https://doi.org/10.1002/er.6031).
- [4] R. Tummala. *Fundamentals of Microsystems Packaging*, USA: McGraw-Hill Education, 2001. <https://www.mhprofessional.com/9780071418072-usa-fundamentals-of-microsystems-packaging>

- [5] C. Yadav and R. R. Sahoo, "Effect of nano-enhanced PCM on the thermal performance of a designed cylindrical thermal energy storage system," *Exp. Heat Transf.*, vol. 34, no. 4, pp. 356–375, 2021. DOI: [10.1080/08916152.2020.1751744](https://doi.org/10.1080/08916152.2020.1751744).
- [6] C. R. Paul. *Introduction to Electromagnetic Compatibility*. Second. (Chapters 10, 5, Appendix B), USA: John Wiley & Sons, Inc., 2006. DOI: [10.1002/0471758159](https://doi.org/10.1002/0471758159). <https://onlinelibrary.wiley.com/doi/book/10.1002/0471758159>
- [7] F. P. Incropera, D. P. DeWitt, T. L. Bergman, and A. S. Lavine. *Fundamentals of Heat and Mass Transfer*. 6th Ed. USA: John Wiley & Sons, Inc., 2007. DOI: [10.1016/j.applthermaleng.2011.03.022](https://doi.org/10.1016/j.applthermaleng.2011.03.022).
- [8] G. Jiang and D. D. Zhou, Technology advances and challenges in hermetic packaging for implantable medical devices, 2009. DOI: [10.1007/978-0-387-98120-8_2](https://doi.org/10.1007/978-0-387-98120-8_2).
- [9] J. M. H. Morales. *Evaluating Biocompatible Barrier Films as Encapsulants of Medical Micro Devices*. France: Université Grenoble Alpes, 2016.
- [10] H. Chen, *et al.*, "Thermal conductivity of polymer-based composites: fundamentals and applications," *Prog. Polym. Sci.*, vol. 59, pp. 41–85, 2016. DOI:[10.1016/j.progpolymsci.2016.03.001](https://doi.org/10.1016/j.progpolymsci.2016.03.001).
- [11] M. Schlesinger and M. Paunovic. *Modern Electroplating*. Fifth Ed. USA; 2011. DOI: [10.1002/9780470602638](https://doi.org/10.1002/9780470602638).
- [12] IEC, IEC 60601-1-2 - Medical electrical equipment - Part 1-2: general requirements for basic safety and essential performance - Collateral Standard: electromagnetic disturbances - Requirements and tests, 2014.
- [13] CISPR, EN 55011:2007 - Industrial, scientific and medical equipment - radio-frequency disturbance characteristics - Limits and methods of measurements, 2007.
- [14] N. B. D. Do, *et al.*, New encapsulation concepts for medical ultrasound probes- A heat transfer simulation study, in: 2019 22nd Eur. Microelectron. Packag. Conf. Exhib. EMPC 2019, Pisa, Italy, 2019. DOI: [10.23919/EMPC44848.2019.8951832](https://doi.org/10.23919/EMPC44848.2019.8951832).
- [15] Stratasys. "Objet30 Prime," *Tech. Datasheet*, p. 3-2 to 3-9, 2016.
- [16] ISO/ASTM, ISO/ASTM 52900-2015: additive manufacturing – General principles – Terminology, 2015.
- [17] Epoxy Technology. "EPO-TEK EJ2189-LV," *Tech. Datasheet*, p. 2, 2017.
- [18] Stratasys. "Biocompatible Clear MED610," *Tech. Datasheet*, p. 2, 2018.
- [19] Humber River Hospital, Preparing for your Transesophageal Echocardiogram (TEE), (2016).
- [20] J. Calvert, F. Duck, S. Clift, and H. Azaimé. "Surface heating by transvaginal transducers, *Ultrasound Obstet., Gynecol.*, 2007. DOI: [10.1002/uog.3973](https://doi.org/10.1002/uog.3973).
- [21] P. Miloro, E. Martin, and A. Shaw, "Temperature elevation measured in a tissue-mimicking phantom for transvaginal ultrasound at clinical settings," *Ultrasound*, vol. 25, no. 1, pp. 6–15, 2017. DOI: [10.1177/1742271X16684529](https://doi.org/10.1177/1742271X16684529).
- [22] National Physical Laboratory, Tissue phantom for assessment of surface temperature of an ultrasonic transducer, Datasheet. (2017).
- [23] Heat Scientific, Heat scientific MCH Metal Ceramic Heater, HS-PS101012Y Datasheet. (2018).
- [24] Aalco. "Aluminium alloy 6082," *Tech. Datasheet*, p. 2, 2019.
- [25] Epoxy Technology. "EPO-TEK T7109-19," *Tech. Datasheet*, p. 2, 2019.
- [26] K. Jagannadham, "Thermal conductivity of copper-graphene composite films synthesized by electrochemical deposition with exfoliated graphene platelets," *Metall. Mater. Trans. B Process Metall. Mater. Process. Sci.*, vol. 43, no. 2, pp. 316–324, 2012. DOI: [10.1007/s11663-011-9597-z](https://doi.org/10.1007/s11663-011-9597-z).
- [27] COMSOL Multiphysics v. 5.3a, *COMSOL Material Library*, Sweden: COMSOL AB, 2018.
- [28] G. Wypych. *Handbook of Polymers*. Second Ed. Toronto, Canada: ChemTec Publishing, 2016. DOI: [10.1016/C2015-0-01462-9](https://doi.org/10.1016/C2015-0-01462-9). <https://www.elsevier.com/books/handbook-of-polymers/wypych/978-1-895198-92-8>
- [29] A. J. T. Teo, *et al.*, "Polymeric biomaterials for medical implants and devices," *ACS Biomater. Sci. Eng.*, vol. 2, no. 4, pp. 454–472, 2016. DOI: [10.1021/acsbiomaterials.5b00429](https://doi.org/10.1021/acsbiomaterials.5b00429).
- [30] S. Sandell, *et al.*, "Enhancement of thermal boundary conductance of metal–polymer system," *Nanomaterials*, vol. 10, no. 4, pp. 670, 2020. DOI: [10.3390/nano10040670](https://doi.org/10.3390/nano10040670).
- [31] S. Babu, K. Manisekar, A. P. S. Kumar, and D. Rajenthirakumar, "experimental study of thermal contact resistance in hardened bearing surfaces," *Exp. Heat Transf.*, vol. 28, no. 2, pp. 189–203, 2015. DOI: [10.1080/08916152.2013.860503](https://doi.org/10.1080/08916152.2013.860503).
- [32] M. Asif and A. Tariq, "Correlations of thermal contact conductance for nominally flat metallic contact in vacuum," *Exp. Heat Transf.*, vol. 29, no. 4, pp. 456–484, 2016. DOI: [10.1080/08916152.2015.1024352](https://doi.org/10.1080/08916152.2015.1024352).
- [33] J. R. Taylor and W. Thompson, An introduction to error analysis: the study of uncertainties in physical measurements, 1997.
- [34] Y. Duan and H. Yang, "Influence of thermal contact resistance of cementing interface on radial heat transfer in wellbore," *Exp. Heat Transf.*, vol. 34, no. 1, pp. 68–84, 2021. DOI: [10.1080/08916152.2020.1715511](https://doi.org/10.1080/08916152.2020.1715511).
- [35] D. Liao, *et al.*, "Oesophageal heat transfer properties indication of segmental blood flow changes during distension," *Neurogastroenterol. Motil.*, vol. 20, no. 4, pp. 298–303, 2008. DOI: [10.1111/j.1365-2982.2007.01031.x](https://doi.org/10.1111/j.1365-2982.2007.01031.x).
- [36] M. Ohashi, S. Kawakami, Y. Yokogawa, and G. C. Lai, "Spherical aluminum nitride fillers for heat-conducting plastic packages," *J. Am. Ceram. Soc.*, vol. 88, no. 9, pp. 2615–2618, 2005. DOI: [10.1111/j.1551-2916.2005.00456.x](https://doi.org/10.1111/j.1551-2916.2005.00456.x).

- [37] Z. Zhu, *et al.*, “Densely packed polymer/boron nitride composite for superior anisotropic thermal conductivity,” *Polym. Compos.*, vol. 39, no. S3, pp. E1653–E1658, 2018. DOI: [10.1002/pc.24615](https://doi.org/10.1002/pc.24615).
- [38] T. Kusunose, T. Yagi, S. H. Firoz, and T. Sekino, “Fabrication of epoxy/silicon nitride nanowire composites and evaluation of their thermal conductivity,” *J. Mater. Chem. A*, vol. 1, no. 10, pp. 3440, 2013. DOI: [10.1039/c3ta00686g](https://doi.org/10.1039/c3ta00686g).
- [39] N. G. Berg, T. Paskova, and A. Ivanisevic, “Tuning the biocompatibility of aluminum nitride,” *Mater. Lett.*, vol. 189, pp. 1–4, 2017. DOI:[10.1016/j.matlet.2016.11.041](https://doi.org/10.1016/j.matlet.2016.11.041).
- [40] M. Qin, *et al.*, “Powder injection molding of complex-shaped aluminium nitride ceramic with high thermal conductivity,” *J. Eur. Ceram. Soc.*, vol. 39, no. 4, pp. 952–956, 2019. DOI: [10.1016/j.jeurceramsoc.2018.11.037](https://doi.org/10.1016/j.jeurceramsoc.2018.11.037).